Analysis of active regions via 3D rendering techniques

David Alexander

Lockheed Martin Solar and Astrophysics Group, Org. H1-12 B/252, 3251 Hanover St., Palo Alto, CA 94304

G. Allen Gary

Space Sciences Lab/ES82, Marshall Space Flight Center/NASA, Huntsville, AL 35812

Barbara J. Thompson

Space Applications Corp., Goddard Space Flight Center/NASA, Greenbelt, MD 20771

Abstract. We analyze coronal X-ray and EUV structures by constructing synthesized images which can be compared with observations. Images are rendered from complete 3D models of multiple fluxtubes. The active region magnetic loop complex is defined using extrapolations of Kitt Peak magnetogram data and a model of coronal heating is used to determine the plasma content of the fluxtubes. Our initial aim is to test these models using an active region with a relatively simple magnetic configuration before progressing to more complicated force-free models. We have identified such an active region which traversed disk center on 26-Nov-96. The modeling of this active region complex as a collection of quasi-static loops indicates that even in an active region displaying a simple potential field configuration the heating of individual loops is far from simple. We investigate how different pressure distributions within the active region loop system affect the emission characteristics and compare the various results with SOHO/EIT and *Yohkoh*/SXT observations.

1. Introduction

EUV and X-ray observations of the solar corona show that it is comprised of three-dimensional magnetic structures appearing primarily in the form of fluxtubes or loops. The relationship between the magnetic field and the heating of these loops requires a knowledge of the field distribution in the corona and an understanding of the coronal response to changes in this distribution. However, none of these theories have been demonstrated to be Because of the large discrepancy between the scales at which the energy dissipation occurs and the scales at which we observe, no direct test of the various coronal heating mechanisms is practical. However, by considering broad classes of heating mechanisms, it is possible to constrain the relevant parameters. We approach the heating problem

in an empirical way by assuming that individual fluxtubes are heated in a manner that is proportional to one or more of the parameters defining the fluxtube, e.g. pressure, length, field strength, current density, etc. (cf. Alexander & Katsev 1996; Gary 1997). In this paper we concentrate on interlacing the different components of the active region simulation and keep the field extrapolation and coronal heating models as simple as possible. Section 2 outlines the different stages of the analysis which are then applied to a specific case in section 3. We end by making some general conclusions in section 4.

2. Simulating an active region

The solar corona is optically-thin to EUV and X-ray radiation. Consequently, any coronal radiation at these wavelengths arriving at a detector is an integrated sum of all of the emitted photons along the line-of-sight. The two-dimensional projections produced by either of the SXT or EIT instruments are then potentially subject to misinterpretations regarding the actual three-dimensional distribution of the emission at the Sun. To model active regions fully requires a knowledge of the 3D coronal magnetic field as well as a knowledge of the mechanism(s) heating the plasma contained by this field. Lacking a direct measure of the coronal field, an understanding of the former requires observations of the photospheric or chromospheric field which then provide the necessary boundary conditions for extrapolation techniques (e.g. Sakurai, 1981). An understanding of the latter can be obtained by comparing the consequences of the various heating models with the observed distributions of plasma parameters. Our approach then can be divided into four distinct stages.

Step 1: Generating the 3D coronal field The magnetic field distribution in the low solar corona is expected to be approximately force-free, satisfying $\nabla \times \underline{B} = \alpha(\underline{r})\underline{B}$, where $\alpha(\underline{r})$ is constant along any given field line. This assumption allows the 3D distribution of coronal field to be reconstructed from the measured photospheric field. The potential field limit ($\alpha = 0$) has zero current and, therefore, limits any study of the heating to wave dissipation mechanisms. However, the reconstruction of such field distributions is well understood, computationally simple and serves to provide some insight into the physics of coronal loop heating. We have implemented the iteration methods of Sakurai (1981) to carry out a potential field extrapolation of active region magnetograms (Gary 1997; Gary, Alexander & Thompson 1998).

Step 2: Generating a fluxtube distribution The basic property of a fluxtube is that the magnetic flux is conserved along its length. In our analysis, we will assume that the fluxtubes have circular cross-sections and that, consistent with observations, no fluxtube expands into an adjacent fluxtube. A consequence of this prescription is that the fluxtube footpoint has to be defined in some reasonably objective fashion. The field lines are selected by a flux strength algorithm applied to the surface distribution of field (see Gary 1997).

For a given field line a basal radius, $r = r_0$, the conservation of magnetic flux then defines the fluxtube, via $r/r_0 = \sqrt{B/B_0}$.

Step 3: Heating the fluxtubes The simplest approach, which we adopt here, is to assume quasi-static equilibrium in constant pressure loops. Since Lorentz forces vanish in the direction of the magnetic field and the force balance equation leads to hydrostatic equilibrium along a given field line, the thermodynamical structure of the loop is determined by the conservation of energy

$$\frac{dF_c(s)}{ds} = A(E_{heat}(s) - E_{rad}(s)) \tag{1}$$

and an equation of state, $p = 2nkT$. Here, s is the coordinate along the $\mathbf{B}$, A is the constant cross-section of the loop, p is the constant pressure, and n the electron density. The classical conductive flux is given by $F_c(s) = -A\kappa_0 T^{5/2}(dT/ds)$ with $\kappa_0 = 8.8 \times 10^{-7}$ (erg cm^{-1}s^{-1}K$^{-7/2}$) and T is the temperature. The optically-thin radiative losses are given by $E_{rad}(s) = n^2\Psi(T)$ with $\Psi(T)$ the emissivity, and $E_{heat}(s)$ is the heat input. Once $E_{heat}(s)$ is specified, equation (1) can be solved to yield a distribution of thermodynamic variables within the fluxtube which is governed by a simple scaling law (cf. Rosner, Tucker & Vaiana 1978 (RTV); Kano & Tsuneta 1995), viz.

$$T_{max} = C\ (pL)^{\delta} \tag{2}$$

where T_{max} is the maximum temperature attained in the loop, L is the loop half-length and C and δ are constants. We will adopt $\delta = 1/3$ in agreement with RTV, although other possibilities will be explored in future works. The distribution of temperature and density throughout the loop is then uniquely determined by a choice of any two parameters from p, L, T_{max}, or E_{heat}.

Our initial approach is to assume the same heating rate for each loop within an active complex and that this rate is directly proportional to the pressure adopted and comparing the emission characteristics of the emitting loop complex with observations we can place constraints on the quasi-static heating assumption.

Step 4: Comparison with imaging observations Once the distribution of plasma parameters is determined it can be folded through a given instrument response function to produce a simulated active region at the wavelength of interest. The goal here is not to reproduce exactly every loop within the active region but to look for a gross agreement which would enable us to differentiate between different physical assumptions within a given model or competing models.

3. Rendering NOAA AR7999

AR7999 traversed disk center on 26 November 1996. The EUV and X-ray images show a relatively simple active region with a bright core of apparently low-lying loop structures within a larger complex of long diffuse loops. Both the white light and magnetogram images support this picture indicating a fairly simple sunspot pair. The leading spot appears as a single uniform structure with negligible current density (T. Metcalf - private communication) while the following spot has a degree of fragmentation and evidence of a significant current density in its southernmost portion.

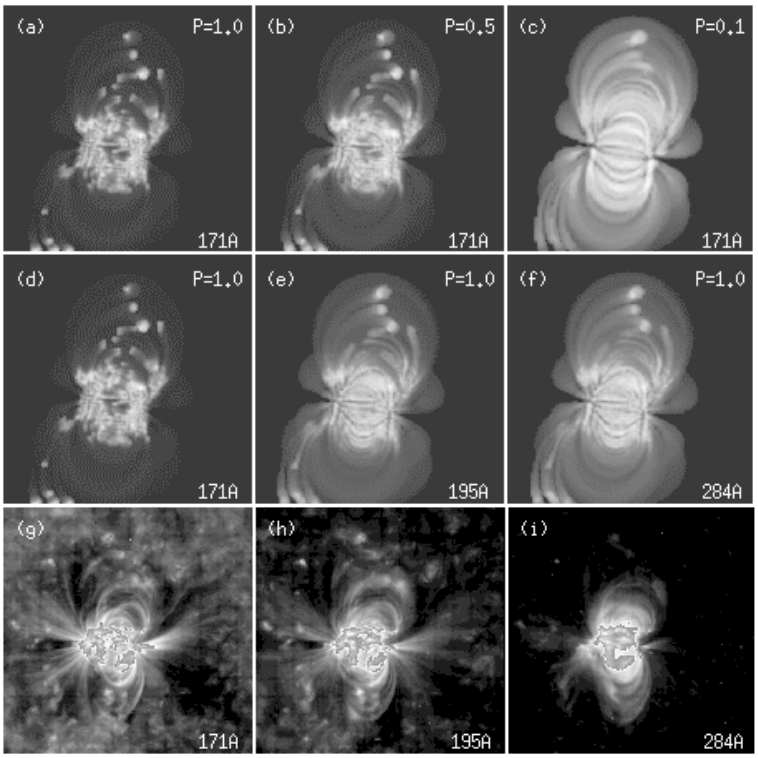

Figure 1. Simulation of AR7999 EIT observations. The top panel shows the simulated Fe IX (171 Å) active region with an assumed pressure of a) 1, b) 0.5 and c) 0.1 dyne cm^{-2}. The middle panel shows the simulated d) Fe IX (171Å), e) Fe XII (195Å) and f) Fe XV (284Å) emission for p = 1 dyne cm^{-2}. The lower panels show the observed active region in the EIT g) Fe IX, h) Fe XII and i) Fe XV lines.

The coronal field distribution was generated using a potential field extrapolation of Kitt Peak magnetogram data. Figure 1 shows the simulated and observed active region in the three coronal EIT lines. The simulated emission takes account of the instrumental response function and was generated in the manner described in the preceeding section. For these assumptions the differences in the emission characteristics of individual loops is due entirely to their length. No attempt was made to reproduce the very diffuse emission pervading the active region which is presumably due to the line-of-sight integral of a number of faint unresolved structures rooted in weak field regions.

The first thing to notice from Figure 1 is that, despite the obvious simplicity of the assumed heating, the simulated active region is a remarkably good representation of the real active region. This preliminary analysis, however, clearly demonstrates that a single pressure is unable to explain the distribution of emission within even this relatively simple active region. The simulated 171Å emission shows that the average pressure of the active region complex lies somewhere between 0.1 and 0.5 dyne cm^{-2}. In addition, a comparison of different

EIT filters shows that different pressure distributions are required in the different temperature regimes (see Gary et al. 1998, for more details). A more realistic approach, where there is a distribution of loop pressures throughout the active region, is currently being considered. In addition, a close examination of the loop structures shows that they deviate significantly from the potential configuration, particularly in the southern half of the active region. This discrepancy can be removed by the addition of currents to the system (Gary et al. 1998)

4. Conclusions

In this paper, we have simulated the 3D coronal emission of an active region. Our simulation incorporated a potential field extrapolation of the photospheric magnetic field and a constant pressure quasi-static heating model. We also assumed that each loop within the active region had the same pressure. Under these simplifying assumptions the distribution of EIT intensity can be parameterized in terms of the loop pressure. The comparison of the simulated emission with that observed provides a basis for comparison with other heating models.

Several other forms of the heating function for these quasi-static loops can be adopted and their relationship to the physical conditions of the active region fluxtube distribution used to determine their role in the heating process (cf. Waljeski et al. 1992). Specifically, by allowing our coronal fluxtubes to be heated according to any one of several mechanisms, we are able to generate a complex of active region loops as would be observed by the various channels of the SOHO/EIT and/or the *Yohkoh*/SXT. The comparison with the relevant data then allows us to determine which of the heating models are favored by the active region corona. Future studies will include linear and non-linear force-free field extrapolations (e.g. Yan & Sakurai 1996) and will test a variety of heating functions to determine which of the physical parameters of the active region contribute most to the heating of coronal loops.

Acknowledgments. This work was supported on by NASA under contracts NAS8-40801 and NAS5-32966 and by a Collaborative Research Grant from NATO CRG940603 (D.A.) and by the NASA office of Solar Physics and MSFC Director's Discretionary Fund (G.A.G.).

References

Alexander, D. & Katsev, S. 1996, *Solar Phys.*, 153, 153

Gary, G. A. 1997, *Solar Phys.*, 174, 241

Gary, G. A., Alexander, D. & Thompson, B. J. 1998, in preparation

Kano, R. & Tsuneta, S. 1995, ApJ, 454, 934

Rosner, R., Tucker, W. H. & Vaiana, G. S. 1978, ApJ, 220, 643

Sakurai, T. 1981, *Solar Phys.*, 69, 343

Waljeski, K., Dere, K. P. & Moses, D. 1992, in *Proceedings of the First SOHO Workshop*, p.281

Yan, Y. & Sakurai, T. 1996, in *Proceedings of Workshop on Measurements and Analyses of 3-D Solar Magnetic Fields.*